The Astrophysical Journal, 783:34 (8pp), 2014 March 1 doi:10.1088/0004-637X/783/1/34

BLUE STRAGGLER MASSES FROM PULSATION PROPERTIES. I. THE CASE OF NGC 6541

G. Fiorentino[1], B. Lanzoni[1], E. Dalessandro[1], F. R. Ferraro[1], G. Bono[2,3], and M. Marconi[4]
[1] Dipartimento di Fisica e Astronomia, Università degli Studi di Bologna, Viale Berti Pichat 6/2, I-40127 Bologna, Italy; giuliana.fiorentino@oabo.inaf.it
[2] Dipartimento di Fisica, Universitá di Roma Tor Vergata, Via della Ricerca Scientifica 1, I-00133 Roma, Italy
[3] INAF-Osservatorio Astronomico di Roma, Via Frascati 33, I-00040 Monte Porzio Catone, Italy
[4] INAF-Osservatorio Astronomico di Capodimonte, Via Moiariello 16, I-80131 Napoli, Italy
Received 2013 November 4; accepted 2013 December 2; published 2014 February 11

ABSTRACT

We used high spatial resolution images acquired with the Wide Field Camera 3 on board *Hubble Space Telescope* to probe the population of variable blue straggler stars (BSSs) in the central region of the poorly studied Galactic globular cluster NGC 6541. The time sampling of the acquired multiwavelength (F390W, F555W, and F814W) data allowed us to discover three WUMa stars and nine SX Phoenicis. Periods, mean magnitudes, and pulsation modes have been derived for the nine SX Phoenicis, and their masses have been estimated by using pulsation equations obtained from linear nonadiabatic models. We found masses in the range 1.0–1.1 $M_\odot$, with an average value of $1.06 \pm 0.09\, M_\odot$ ($\sigma = 0.04$), significantly in excess of the cluster main-sequence turn-off mass ($\sim 0.75\, M_\odot$). A mild trend between mass and luminosity seems also to be present. The computed pulsation masses turn out to be in very good agreement with the predictions of evolutionary tracks for single stars, indicating values in the range ~ 1.0–$1.2\, M_\odot$ for most of the BSS population, in agreement with what was discussed in a number of previous studies.

Key words: binaries: general – blue stragglers – globular clusters: individual (NGC 6541) – stars: fundamental parameters

Online-only material: color figures

1. INTRODUCTION

Dense stellar environments like Galactic globular clusters (GCs) are populated by a large variety of *exotica*, including blue straggler stars (BSSs), X-ray binaries, millisecond pulsars, and cataclysmic variables (see Bailyn 1995; Pooley & Hut 2006; Paresce et al. 1992; Bellazzini et al. 1995; Ferraro et al. 2001; Ransom et al. 2005; Freire et al. 2008). Among them, BSSs certainly are the most numerous. They were discovered by Sandage (1953) in the outer regions of the Galactic GC M3, and since then they have been detected not only in GCs (see Piotto et al. 2004; Leigh et al. 2011), but also in open clusters (Mathieu & Geller 2009) and dwarf galaxies (Mateo et al. 1995; Mapelli et al. 2007; Monelli et al. 2012).

In the optical color–magnitude diagram (CMD) BSSs are bluer and brighter than the main-sequence (MS) turn-off (TO) stars, defining a sequence that typically spans more than 2 mag above the cluster TO. Hence, they mimic a younger stellar population with masses larger than normal cluster stars. Indeed, masses of the order of $M = 1.0$–$1.7\, M_\odot$ have been estimated by direct measurements, although with large uncertainties (Shara et al. 1997; Gilliland et al. 1998; De Marco et al. 2005).

The origin of BSSs is still a matter of debate. They could originate from collision-induced mergers, most likely in dense stellar environments (Hills & Day 1976; Leonard 1989), or by mass exchange in primordial binary systems (McCrea 1964; Zinn & Searle 1976; Knigge et al. 2009; Ferraro et al. 2006a, 2006b). These two scenarios can possibly coexist within the same cluster (Ferraro et al. 1995, 2009). Independently of their formation mechanism, BSSs are the brightest among the most massive stars in the host cluster and therefore are ideal tools to probe the dynamical evolution of stellar systems. Indeed, the observed shape of their radial distribution within the cluster has been recently used to define the so-called *dynamical clock* (Ferraro et al. 2012), able to rank GCs on the basis of the dynamical stage reached. Since the engine of such a clock is dynamical friction and since the dynamical friction efficiency directly depends on the object mass, an accurate determination of BSS masses is of paramount importance for the calibration of such a clock.

Very interestingly, BSSs cross the faint extension of the classical instability strip (IS), where they are observed as SX Phoenicis (SXP) stars (see Pych et al. 2001; Jeon et al. 2003, 2004; McNamara 2011; Arellano Ferro et al. 2011). These objects show a photometric variability on very short periods ($P \lesssim 0.1$ days) and can be unstable for radial and nonradial pulsation. Hence, their pulsation properties can be used to estimate their masses. The Petersen's diagram (period ratio versus the longer period; Petersen 1978; Stellingwerf 1978; Gilliland et al. 1998), which is largely used for variable stars pulsating simultaneously in different modes, is very little sensitive to the mass in the period range typical of SXPs. However, these variables follow the classical pulsation equation, relating the observed period to the intrinsic stellar parameters such as mass, luminosity, and effective temperature $P(M,\ L,\ T_{\rm eff})$, for any given pulsation mode and chemical composition. This relation can indeed be used to estimate the star mass, once the full set of variables is observed and/or assumed (Stellingwerf 1979; Da Costa et al. 1986; Marconi et al. 2004; Caputo et al. 2005; Fiorentino et al. 2006). For a precise determination of the pulsation equations, a complete theoretical scenario using a nonlinear and nonadiabatic approach, also accounting for the convection, should be defined (Bono et al. 1997; Fiorentino et al. 2002; Marconi et al. 2005). This would be able to fully describe the pulsation properties of SXPs, including their amplitudes and the red (cold) boundary of the IS. However, such a theoretical framework is still missing due to the huge amount of computation time necessary to integrate conservation equations for these high

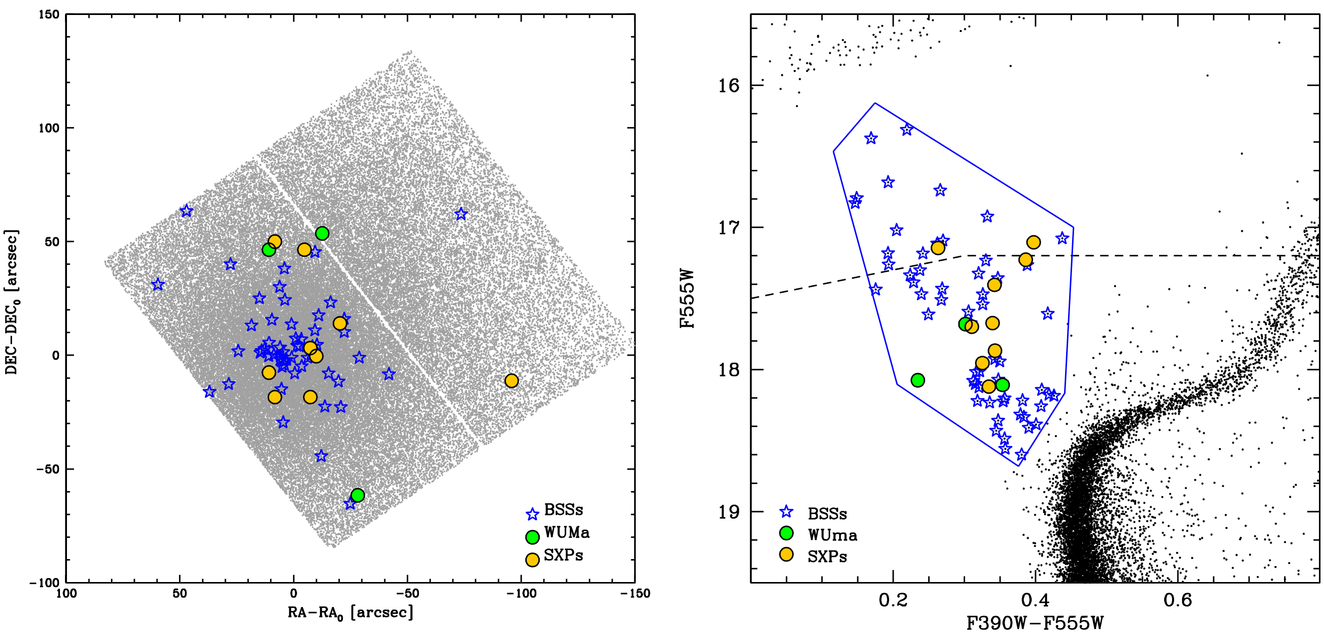

Figure 1. Left: map of the WFC3 data. The location of the selected BSSs is highlighted: blue starred symbols mark nonvariable BSSs, green and orange circles indicate WUMa and SXP BSSs, respectively. Most of the selected BSSs are located in chip 1, where the cluster center is also positioned. Right: (F555W, F390W−F555W) CMD of NGC 6541 zoomed in on the BSS region. The box used to select the BSS population is shown with blue contours. Nonvariable BSSs are marked as blue starred symbols, while variable BSSs are highlighted with green (WUMa) and orange (SXP) filled circles. The saturation limit of our data set is also marked for reference (dashed line).

(A color version of this figure is available in the online journal.)

gravity pulsators. Nevertheless, theoretical models based on a radial, linear, nonadiabatic approach to the stellar pulsation have been shown to reproduce quite confidently the SXP periods and the blue (hot) boundary of the IS (Stellingwerf 1979; Gilliland et al. 1998; Santolamazza et al. 2001), thus supporting the use of these approximated pulsation equations for the mass estimate. Attempts to estimate SXP masses have been performed using the pulsation equation based on Jorgensen & Hansen (1984) linear theoretical models, and masses from about 1.5 $M_\odot$ up to twice the MS TO mass have been obtained for a sample of BSSs in NGC 5053 (Nemec et al. 1995).

In the present paper we use linear and nonadiabatic theoretical pulsation models from Santolamazza et al. (2001) to estimate the mass of a sample of BSSs pulsating as SXPs in the Galactic GC NGC 6541. This is an old (13.25 ± 1 Gyr; Dotter et al. 2010) and metal-poor ([Fe/H] = −1.76 ± −0.02; Lee & Carney 2002) GC with an extended blue horizontal branch (Dotter et al. 2010). It is located at 3 kpc from the Galactic center and is classified as a post-core-collapse cluster (Harris 1996). Here new *HST*/WFC3 (Wide Field Camera 3 on *Hubble Space Telescope*) data are used to detect variable BSSs in the central region of NGC 6541. We found a sizable sample of this exotic population, and we discuss the mass determination for nine SXP pulsating BSSs.

The paper is organized as follows. The *HST* data set and the data reduction procedure are described in Section 2. The BSS selection and their short-period variability study are described in Section 3. In Section 4 we present the method adopted to discriminate the pulsation mode of the nine selected SXPs, whereas in Section 6 we derive their mass. A discussion section closes the paper.

2. OBSERVATIONS AND DATA REDUCTION

The data set presented in this paper has been acquired using the UVIS channel of the *HST*/WFC3 on 2012 February 24 (PI: F. R. Ferraro, GO: 12516). The cluster is centered in chip 1 (see Figure 1, left panel). The data set consists of 12 F390W, 10 F555W (narrow *V*), and 13 F814W (wide *I*) frames. Each frame has been integrated for an exposure time of 348 s, 150 s, and 348 s, respectively. The observing strategy includes a small dithering of a few pixels to correct CCD blemishes, artifacts, and false detections. The three different filters were alternated during each orbit to optimize the final total exposure time.

The data reduction has been performed using DAOPHOT/ALLSTAR/ALLFRAME (Stetson 1987, 1994) on flat-fielded and bias-subtracted (_flt) images once the pixel area map corrections were accounted for. The point-spread functions (PSFs) were derived on chip 1 and 2 separately using the brightest, isolated and nonsaturated stars. Typically, more than 600 stars were selected. These PSFs were used to perform ALLSTAR photometry in each frame. The obtained individual star lists have been combined using DAOMATCH in a single master list to run ALLFRAME. In this master list only stars appearing in at least 20 out of 35 images were included. Finally, the ALLFRAME output star lists were combined using DAOMASTER for each filter. For each star, we have homogenized the different magnitudes (e.g., Ferraro et al. 1991, 1992) to obtain their mean magnitudes and the corresponding time series. The final list includes 72,616 stars.

In order to calibrate instrumental F390W, F555W, and F814W magnitudes in the VEGAMAG photometric system, we have followed the procedure described in Dalessandro et al. (2013), which includes charge transfer efficiency correction for the WFC3 camera. A portion of the resulting (F555W, F390W−F555W) CMD, zoomed in on the BSS region, is shown in Figure 1 (right panel). By following the same paper and according to the estimate of the UVIS channel performance, we have also computed the saturation threshold of our photometry. Following the instructions of the WFC3 Data Handbook, we used 72,000 e$^-$ as the value of the central pixel saturation, and we adopted an aperture of 1×1 pixel for the encircled energy in the three filters: EE (F814W) = 0.149, EE (F555W) = 0.184, and EE (F390W) = 0.180. Then the flux close to saturation was determined and transformed into magnitudes by applying the same equations used to calibrate our photometry in the *HST* VEGAMAG photometric system. The resulting saturation threshold is marked in Figure 1 (right panel, dashed line).

Finally, to obtain a precise absolute astrometric solution, we first accounted for geometric distortion following the prescriptions discussed in the WFC3 Data Handbook. Then the instrumental positions of our stars have been cross-correlated with a wide-field catalog (P. B. Stetson 2013, private communication) previously reported to the absolute astrometric system using the stars in common with the Guide Source Catalogue 2.3 (GSC2.3), by means of CataXcorr (developed by P. Montegriffo at the INAF-Bologna Observatory; see also Dalessandro et al. 2011). Both the WFC3 and the wide-field catalogs will be used in a forthcoming paper to properly determine the center and density profile of NGC 6541 and to constrain the mass and luminosity functions of this cluster.

3. BLUE STRAGGLER STAR SELECTION AND VARIABILITY SEARCH

The BSS population has been selected on the basis of the star location in the CMD (as objects bluer and brighter than the MS TO), with conservative color and magnitude limits aimed at reducing at most the contamination from stellar blends near the MS TO and the subgiant branch. In addition, a simultaneous check of the (F555W, F390W−F555W) and the (F555W, F555W−F814W) planes has been performed, and only stars located in the "appropriate" region in both CMDs have been selected as fiducial BSSs, following the general approach routinely adopted in previous papers (Ferraro et al. 2006b; Dalessandro et al. 2008). The resulting shape of the BSS selection box in the (F555W, F390W–F555W) plane is shown with blue contours in the right panel of Figure 1. The final sample consists of 70 BSSs spanning ∼2 mag in the F555W pass band and approaching the horizontal branch luminosity. The spatial distribution of these stars within NGC 6541 is shown in Figure 1 (left panel), revealing that they are well segregated in the cluster center (as quoted by Harris 1996, 2010 version).

As apparent from Figure 1 (right panel), 16 stars fall above the saturation threshold. However, all variable BSSs (green and orange circles; see below), which are the main targets of this study, are either below or very close to the saturation limit. Hence, they are marginally affected by the photometric saturation. It is worth mentioning that, while possible variability signals may be hidden by saturation effects at brighter magnitudes, the most luminous BSSs are so blue that they unlikely cross the pulsation IS.

Our data sampling was collected within 13 *HST* orbits and consists of 35 images over a time interval of about 7 hr. However, thanks to the high photometric accuracy possible with *HST* (with errors $\sigma_{\rm F390W} - \sigma_{\rm F555W} - \sigma_{\rm F814W} \lesssim 0.015$ mag at the BSS magnitude levels), it has been possible to perform a variability study and search for variable BSSs with short periods and relatively large amplitudes (e.g., $A_{\rm F555W} \gtrsim 0.05$ mag), as already done for the case of NGC 362 (Dalessandro et al. 2013).

To this end, we have performed a Fourier time series analysis for all the selected BSSs in the three filters simultaneously by using GRaphical Analyzer of TIme Series (GRATIS, developed by P. Montegriffo at the INAF-Bologna Observatory; see Clementini et al. 2000; Fiorentino et al. 2010a, 2010b). In particular, we have used low-order Fourier coefficients to match the light curves in each pass band as a function of the phased Heliocentric Julian Date. Only those stars showing variability with the same period within 1% in all of the three filters were considered as bona fide variables. In particular, out of the 70 selected BSSs, 9 stars with period smaller than 0.1 days have been identified as SXPs and 3 stars with period longer than 0.1 days were classified as WUMa stars. It is worth noticing that the detected sample of variable stars is far from complete.

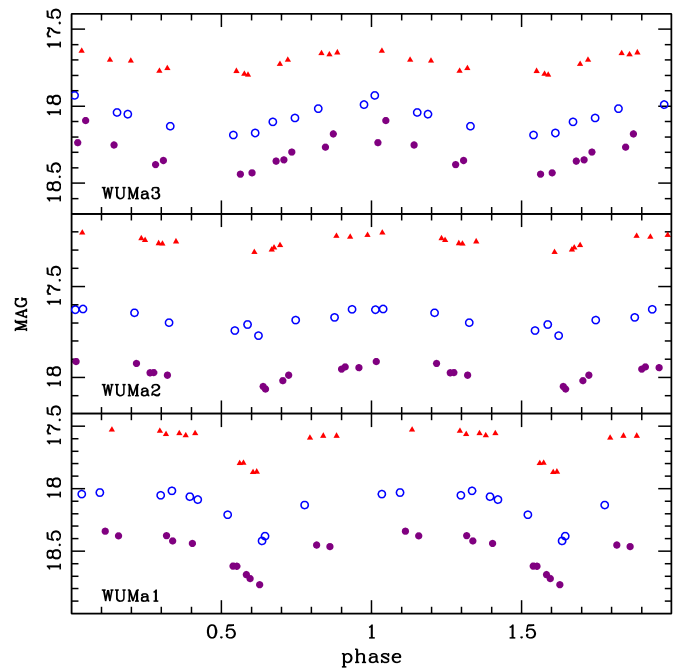

Figure 2. Phased light curves for the WUMa stars detected within our BSS sample. Different filters are color coded in each panel: purple light curve is for the F390W pass band, blue for the F555W, and red for the F814W.

(A color version of this figure is available in the online journal.)

The phased light curves of the three WUMa stars are shown in Figure 2 for the three filters. We remember here that WUMa stars are eclipsing binary systems. WUMa1 shows a not very sinusoidal behavior, with a flattening of the light curve at bright magnitudes due to the contribution of both the companions. The remaining two WUMa stars show, instead, a sinusoidal light curve typical of two very close components in a binary system. Our sample of SXPs shows sinusoidal light curves (see Figures 3–5), as expected in the case of an almost adiabatic behavior with large amplitudes. Despite the modest sampling of our data, we stress here that our classification of stars as SXPs is fully supported by their pulsation properties, e.g., they follow a very tight and well-defined period–luminosity (PL) relation (see Section 4).

Their amplitudes range from 0.06 to 0.39 mag in the F555W filter, and their periods vary from 0.032 to 0.065 days. We stress here that, due to both the photometric errors and the limited temporal sampling of our data, only high-amplitude variations can be detected, and our SXP sample is therefore far from complete. In addition, it is not possible to firmly assess the existence of more than one frequency, and in turn mixed-mode pulsators cannot be solidly recognized.

We derived the mean magnitudes of the detected variable stars using the truncated Fourier series that best match the data. The mean instrumental magnitudes were then calibrated using

Table 1
Parameters of the Variable BSSs Detected in NGC 6541

ID	$\alpha_{J2000.0}$ (deg)	$\delta_{J2000.0}$ (deg)	Period (days)	Epoch (−2455900)	A_{F390W} (mag)	A_{F555W} (mag)	A_{F814W} (mag)	⟨F390W⟩ (mag)	⟨F555W⟩ (mag)	⟨F814W⟩ (mag)	$\langle M/M_{\odot}\rangle$
WUMa1	272.014	−43.702	0.26 ± 0.04	80.850	0.45	0.45	0.34	18.46	18.11	17.62	”
WUMa2	271.999	−43.732	0.20 ± 0.02	81.450	0.14	0.12	0.09	17.98	17.68	17.26	”
WUMa3	272.005	−43.700	∼0.44 ± 0.10[a]	80.850	0.29	0.23	0.16	18.31	18.08	17.72	”
SXP1[F]	272.002	−43.711	0.050 ± 0.001	80.970	0.29	0.26	0.16	18.01	17.67	17.21	1.03 ± 0.15
SXP2[FO]	272.013	−43.701	0.0461 ± 0.003	80.959	$\gtrsim$0.12	0.13	0.06	17.75	17.40	16.90	1.27 ± 0.18[F]–1.07 ± 0.16[FO]
SXP3[F]	272.007	−43.714	0.0649 ± 0.004	80.924	$\gtrsim$0.39	0.44	0.25	17.61	17.20	16.76	1.13 ± 0.17
SXP4[F]	272.006	−43.715	0.041 ± 0.003	80.956	$\gtrsim$0.06	0.07	0.03	18.28	17.95	17.49	1.00 ± 0.15
SXP5[F/FO]	272.007	−43.720	0.065 ± 0.002	80.980	0.27	0.26	0.12	17.50	17.11	16.55	1.23 ± 0.18[F]–1.06 ± 0.16[FO]
SXP6[F]	272.014	−43.717	0.0425 ± 0.001	81.008	0.23	0.20	0.12	18.01	17.70	17.27	1.11 ± 0.16
SXP7[F]	272.013	−43.720	0.032 ± 0.001	80.970	$\gtrsim$0.10	0.13	0.04	18.46	18.12	17.65	1.05 ± 0.15
SXP8[F]	272.008	−43.702	0.046 ± 0.002	80.985	0.10	0.08	0.05	18.21	17.87	17.36	0.98 ± 0.15
SXP9[FO]	271.973	−43.718	0.059 ± 0.003	81.015	0.42	0.29	0.15	17.41	17.14	16.66	1.27 ± 0.19[F]–1.09 ± 0.16[FO]

Notes. Name, coordinates, period, epoch, amplitude, and mean magnitude for the WUMa and SXP stars identified in the BSS sample of NGC 6541. For the nine SXPs, also the likely pulsation mode (F/FO) and the estimated pulsation mass are indicated (the latter corresponds to the average among the values obtained in the three filters; see Section 5). For those stars with uncertain mode classification, we have listed two possible values for the mass as computed using F or FO PL relations.
[a] This is the best period that matches our data in the range 0.01–0.9 days. However, we note that our time sampling covers only 0.3 days; thus, this value may be very uncertain.

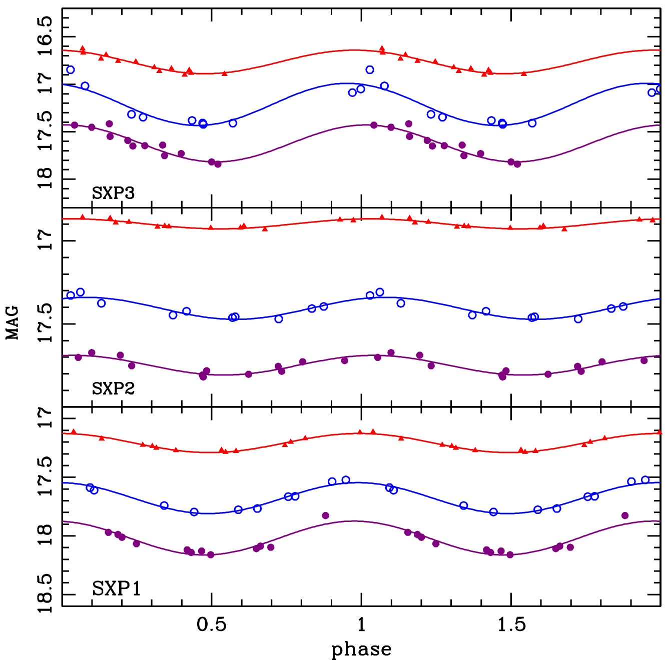

Figure 3. Phased light curves for three SXPs detected in our BSS sample. The color code is as in Figure 2.

(A color version of this figure is available in the online journal.)

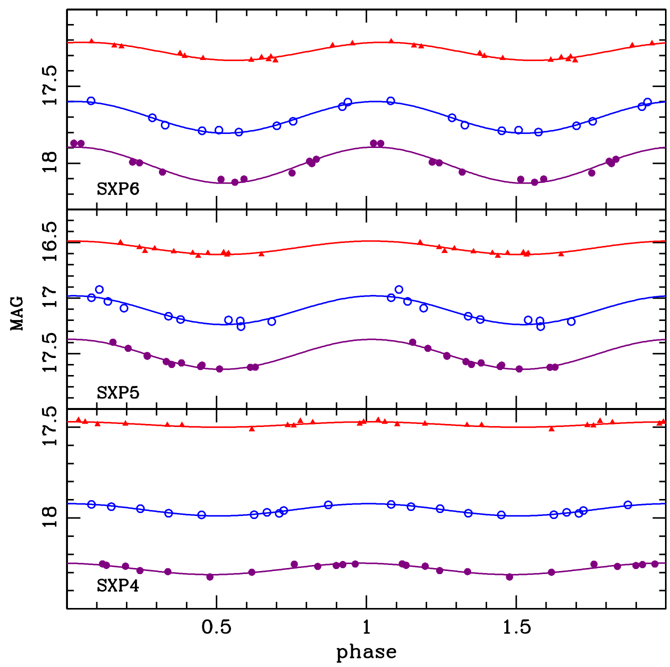

Figure 4. Same as in Figure 3 for three other SXP BSSs.

(A color version of this figure is available in the online journal.)

the same method adopted for nonvariable stars and described in the previous section. The intensity-averaged mean magnitudes, periods, amplitudes, and epochs (time at the maximum of the light curve) are listed in Table 1, together with the star coordinates. The position in the CMD of the detected SXP and WUMa stars, plotted according to the values given in Table 1, is shown in Figure 1 (right panel).

4. PULSATION MODE IDENTIFICATION

In order to estimate the star mass from the pulsation equation, the first step is to determine the pulsation mode of the investigated variables. For well-known pulsating stars crossing the IS, such as RR Lyrae, the first overtone (FO) mode pulsators show a more sinusoidal light curve with respect to the fundamental (F) mode pulsators. Moreover, the FO amplitudes are typically smaller than the F ones. Hence, the pulsation mode can be easily estimated from the morphology of the light curve. In those cases where these general rules are not easily applied, as for SXP stars and anomalous Cepheids, more detailed pulsation properties can also be adopted, e.g., the location in the PL plane when variable stars are located at the same distance (Marconi et al. 2004; Fiorentino et al. 2006). We note that in recent years, the SXP PL relation has been accurately investigated in several Galactic GCs (e.g., Pych et al. 2001; Jeon et al. 2003, 2004; McNamara 2011; Arellano Ferro et al. 2011, and reference therein) and in dwarf galaxies (e.g., LMC, Fornax, Carina; see Vivas & Mateo 2013) to determine the distance of the host stellar system. Here,

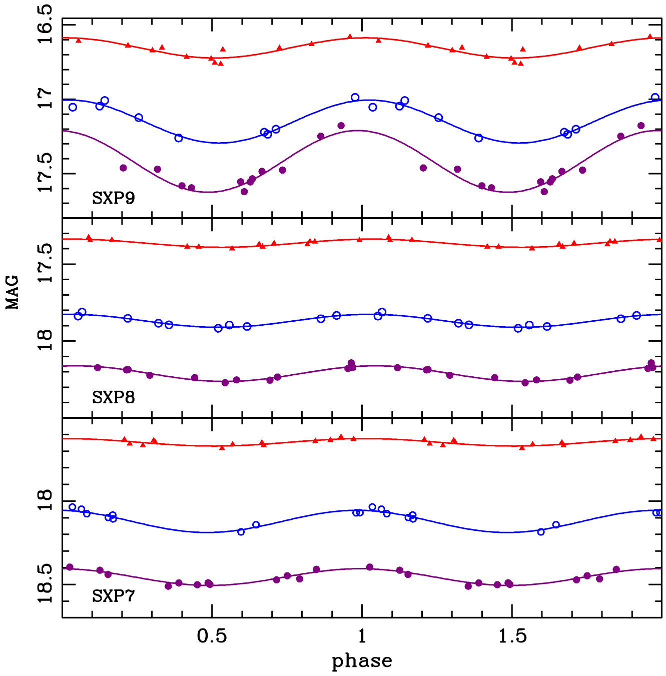

Figure 5. Same as in Figure 3 for three other SXP BSSs.
(A color version of this figure is available in the online journal.)

instead, we use it only to determine the pulsation mode of our SXP sample, which is needed to estimate the SXP pulsation mass (see Section 5).

Empirical and theoretical results suggest significantly different periods for the F and the FO mode pulsations in SXPs, with a ratio $P_{FO}/P_F \sim 0.783$ (Santolamazza et al. 2001; Jeon et al. 2003; Arellano Ferro et al. 2011; Pych et al. 2001). Thus, the two pulsation modes can be confidently distinguished in the period–absolute magnitude plane. Indeed, abundant populations of SXPs in metal-poor GCs (21 SXPs with [Fe/H] = −2.10 in M53, and 24 SXPs at [Fe/H] = −1.94 in M55; Arellano Ferro et al. 2011; Pych et al. 2001, respectively) define two separate sequences well fitted, respectively, by the PL relation derived for F mode pulsators (solid lines in Figure 6) and by the same relation shifted under the assumption $P_{FO}/P_F = 0.783$ (dotted lines).[5] We therefore used these relations to infer the pulsation mode of our SXPs, by assuming a reddening $E(B-V) = 0.14$ mag (Cardelli et al. 1989) and a distance modulus $\mu_0 = 14.29$ mag (Lee & Carney 2002) for NGC 6541.

As shown in Figure 6, most of our variables follow the F mode PL relation in both the F555W (V) and the F814W (I) bands, with the possible exception of three stars, namely, SXP2, SXP5, and SXP9. SXP2 and SXP9 seem to well follow the PL relations for FO mode pulsators in all of the three filters. The case of SXP5 is more ambiguous, this star being located close to the F mode PL relation in F390W and F555W pass bands, whereas it follows better the FO mode PL relation in the F814W filter. Here it is worth noticing that, since SXP5 has a quite large amplitude and its light curve is not fully covered by our data, its mean magnitude estimates may be not very accurate. For this reason, in the following discussion we will consider that SXP5 can be classified as either an F or FO pulsator.

[5] These relations have been obtained in the Johnson Kron–Cousins photometric system; we do not expect any large difference when using F555W and F814W magnitudes as in the case of classical Cepheids (Fiorentino et al. 2013).

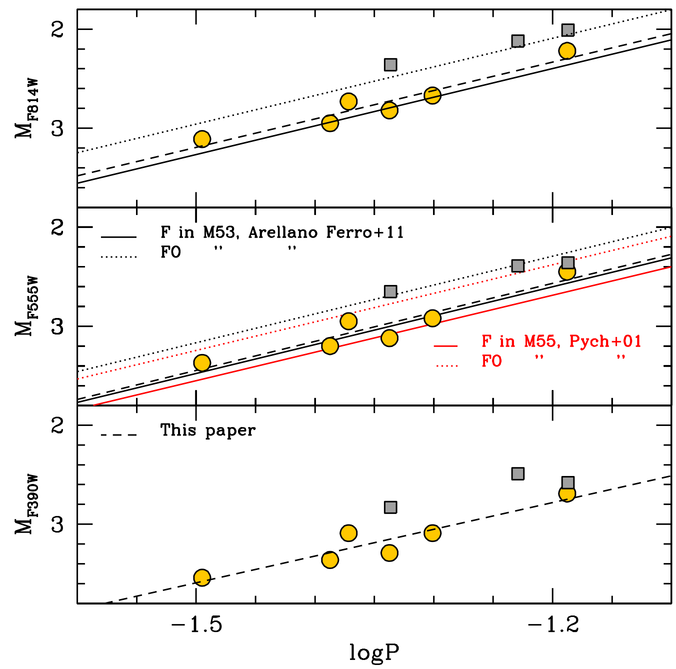

Figure 6. Location of the detected SXP BSSs (orange circles) in the period–absolute magnitude plane, for the three available pass bands under the assumption of a reddening $E(B-V) = 0.14$ mag and a distance modulus $\mu_0 = 14.29$ mag (see Lee & Carney 2002). Orange circles and gray squares represent F and FO pulsators, respectively. The solid lines represent the PL relations derived for the F mode pulsators observed in M53 (black; Arellano Ferro et al. 2011) and in M55 (red; Pych et al. 2001). The dotted lines correspond to these relations shifted assuming $P_{FO}/P_F = 0.783$, and they mark the loci of the FO pulsators. The dashed lines represent the best fits to our data, derived by using only the likely F pulsators (see Section 4 for details).
(A color version of this figure is available in the online journal.)

Table 2
PL Relations for Fundamental Mode Pulsators

Filter	α	β	σ
M_{F390W}	−0.46	-2.70 ± 0.51	0.10
M_{F555W}	−0.95	-2.93 ± 0.53	0.11
M_{F814W}	−1.11	-2.87 ± 0.42	0.09

Notes. Numerical coefficients of the derived PL relations expressed as MAG = $\alpha + \beta \times \log P$. The last column quotes the rms scatter of each relation.

Finally, we found a quite good agreement (in terms of both the slopes and the zero points) between the linear fit to our likely F pulsators (dashed lines in Figure 6 and Table 2) and the relations quoted by Pych et al. (2001) and Arellano Ferro et al. (2011). Hence, we can reasonably use our data to determine, for the first time, the PL relation of SXPs in the F390W band (see bottom panel of Figure 6 and Table 2).

5. PULSATION MASSES

Once the pulsation modes of our SXP sample have been determined (Section 4), we estimate the BSS mass through pulsation equations $P(M, L, T_{eff})$ derived from the linear and nonadiabatic pulsation models of Santolamazza et al. (2001) for the first two modes. In that paper, the authors present a grid of models assuming three values for the star mass (1.0, 1.2, and 1.4 $M_\odot$) and two different metallicities ([Fe/H] = −2.2 and −1.3 dex) that bracket the iron abundance of NGC 6541 ([Fe/H] = −1.76; Lee & Carney 2002). For each mass, several

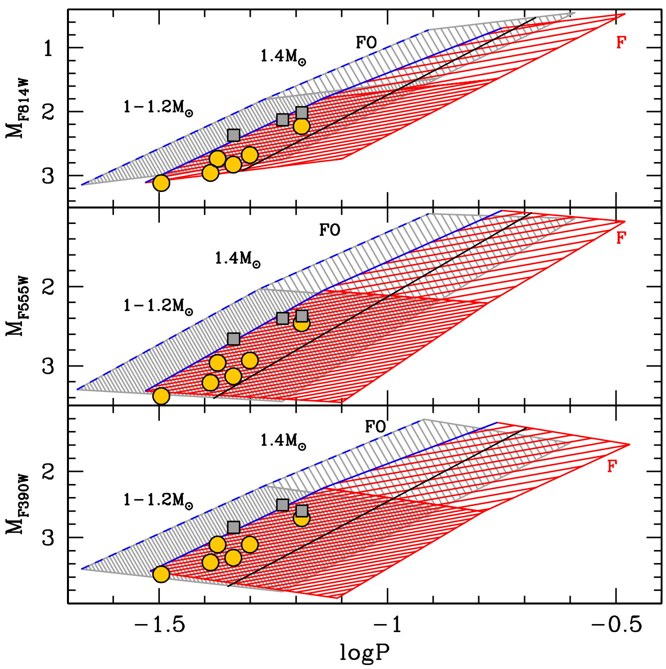

Figure 7. Grids of linear nonadiabatic models (from Santolamazza et al. 2001) in the period–absolute magnitude plane for the available set of filters. Red and gray colors correspond to models computed for F and FO mode pulsators, respectively. Narrow and large shadings correspond to different masses: 1.0–1.2 $M_\odot$ and 1.4 $M_\odot$, respectively. The blue lines represent the theoretical fundamental (solid) and first overtone (dashed) blue edges of the IS. The black solid lines mark the empirical red edge of the IS adopted "ad hoc" for deriving the theoretical PL relations; see the text for details. SXPs are shown for comparison with the same symbols as in Figure 6.

(A color version of this figure is available in the online journal.)

luminosity levels are adopted. The models also span a large range in effective temperatures to reproduce the extension of the IS. However, the major limit of the adopted models is that they do not account for the efficiency of the convection flux during the pulsation. This becomes especially important at cold effective temperatures ($T_{\rm eff} \sim 6000$ K for the SXP mass range), where convection can balance the temperature gradient in the stellar envelope, with the final effect of quenching the stellar pulsation. This means that the linear nonadiabatic approach is unable to predict the location of the red boundary of the IS, and the explored temperatures cover a large range arbitrarily fixed by the authors. To overcome this limitation, we decide to adopt the *observed* red boundary of the IS, which seems to be a quite reasonable assumption.

In order to compare the models with our data, we have transformed the theoretical luminosities and effective temperatures into the VEGAMAG *HST* photometric system, as described in Fiorentino et al. (2013). The region covered by the grid of F and FO models in the PL plane is shown in Figure 7 for the three filters. The red and gray colors indicate the F and FO modes, respectively, and the two different shadings indicate models with masses 1.0–1.2 and 1.4 $M_\odot$. These regions become narrower and steeper moving toward longer wavelengths (from F390W to F814W). Our observations are shown for comparison and clearly define a very narrow region in period at fixed luminosity, whereas the models span a larger period range. As mentioned above, this is a fictitious consequence of using a linear nonadiabatic approach. To better constrain the models, the red boundary of the IS is empirically fixed at *de-reddened* colors (F555W−F814W) ∼ 0.4 mag (see the black lines shown

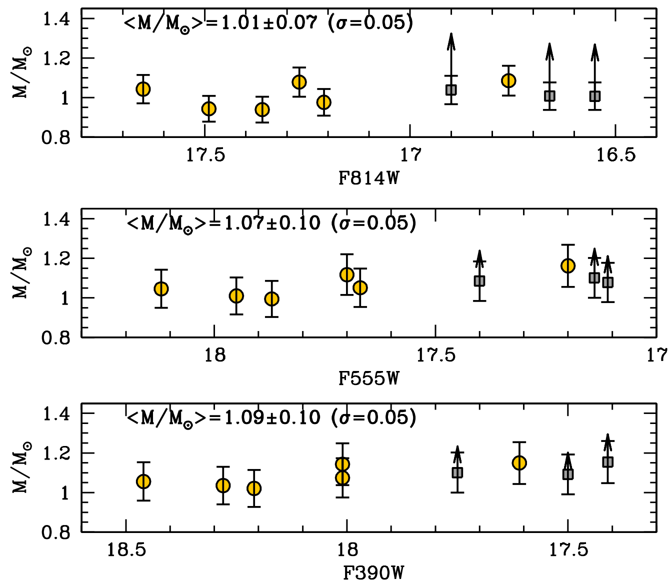

Figure 8. Pulsation masses as a function of magnitude for the nine SPX BSSs, estimated from the pulsation equations listed in Table 3 (see Section 5 for details). The mean values of the mass obtained in the three pass bands are labeled in each panel together with their error and their standard deviation. Symbols are the same used in Figure 6. Arrows point at the mass values derived when F PL relations are used for stars with uncertain mode classification.

(A color version of this figure is available in the online journal.)

Table 3
Pulsation Equations Used to Estimate the Star Mass

Filter	α	β	γ	δ	σ
			F mode		
M_{F390W}	0.13	-0.18 ± 0.04	-0.38 ± 0.13	0.02 ± 0.01	0.04
M_{F555W}	0.05	-0.20 ± 0.04	-0.46 ± 0.13	0.01 ± 0.01	0.04
M_{F814W}	−0.27	-0.33 ± 0.05	-0.89 ± 0.15	0.01 ± 0.01	0.03
			FO mode		
M_{F390W}	0.13	-0.14 ± 0.03	-0.26 ± 0.08	0.01 ± 0.01	0.04
M_{F555W}	0.04	-0.17 ± 0.03	-0.34 ± 0.09	0.01 ± 0.01	0.04
M_{F814W}	−0.31	-0.29 ± 0.03	-0.77 ± 0.11	0.01 ± 0.01	0.03

Note. Numerical coefficients of the pulsation equations derived from linear nonadiabatic models and expressed as $\log M/M_\odot = \alpha + \beta \times \mathrm{MAG} + \gamma \log P + \delta \log Z/Z_\odot$.

in Figure 7), which corresponds to the location in the CMD of the reddest SXPs *observed* in our sample, as well as in that of NGC 5024 (Arellano Ferro et al. 2011) with similar metallicity.

To construct the pulsation equations, we therefore used only the models bluer than this limit and, owing to the limited range in color, we also neglected the temperature dependence. Within these assumptions, for each selected filter and pulsation mode, the grid of available models allowed us to derive pulsation equations of the form $\log M/M_\odot = \alpha + \beta \times \mathrm{MAG} + \gamma \log P + \delta \log Z/Z_\odot$, with the values of the coefficients listed in Table 3.

While the visual inspection of Figure 7 already suggests that the observed variable BSSs have masses consistent with 1.0–1.2 $M_\odot$, the derived relations have been used to estimate the mean mass and the dispersion for each star using the observational data in the three pass bands. The results are listed in Table 1 and summarized in Figure 8, where masses are plotted as a function of magnitudes in the three pass bands and error bars are estimated from the photometric uncertainty on the mean magnitudes and the dispersion σ of the adopted relations (last column of Table 1). In each panel we also give the mean mass value with its error computed on the whole sample, assuming SXP2, SXP5, and SXP9 as FO pulsators. The standard deviation is also indicated to highlight the very good stability of the data around the mean.

Given the large uncertainty in the mode classification, we have estimated the masses for SXP2, SXP5, and SXP9 also using the F mode classification, and the results are listed in Table 1. Moreover, the arrows in Figure 8 start at the mass values obtained assuming SXP2, SXP5, and SXP9 as FO pulsators and end at those computed adopting the F mode classification. When we assume all the stars as F pulsators, the mean mass values listed in each panel of Figure 8 slightly increase together with their standard deviation, i.e., $\langle M/M_{\odot}(\mathrm{F390W})\rangle = 1.13 \pm 0.10 (\sigma = 0.10)$, $\langle M/M_{\odot}(\mathrm{F555W})\rangle = 1.12 \pm 0.10 (\sigma = 0.10)$, and $\langle M/M_{\odot}(\mathrm{F814W})\rangle = 1.10 \pm 0.08 (\sigma = 0.15)$.

6. DISCUSSION AND CONCLUSIONS

We have used linear nonadiabatic pulsation models (Santolamazza et al. 2001) to estimate the mass of the detected SXP BSSs as a function of their observed mean magnitude, period, and metallicity. As expected, we found that all of the investigated SXP BSSs have (pulsation) masses larger than the stellar mass at the MS TO ($\sim$0.75 $M_{\odot}$), as determined from α-enhanced evolutionary tracks at the cluster metallicity, computed from the BASTI database (Pietrinferni et al. 2004). Within the errors, the obtained results are compatible with an average mass $\langle M/M_{\odot}\rangle \sim 1.06 \pm 0.09 (\sigma = 0.04)$. However, Figure 8 shows a mild trend between mass and luminosity, especially if considering the two pass bands (F555W and F390W) with the highest photometric accuracy (F814W, instead, is significantly more affected by saturation problems). This is best appreciated in Figure 9, where we have grouped the nine SXPs in three magnitude bins and computed their average pulsation mass (see the horizontal black segments and the corresponding labels in the figure). This trend is even stronger when we classify the whole sample of SXPs as formed by F pulsators. In fact, the mean mass in each magnitude bin would be 1.01, 1.14, and 1.21 $M_{\odot}$, going from faint to brighter magnitudes.

In the same Figure 9, the position in the CMD of our SXP BSSs is compared to that of α-enhanced evolutionary tracks (Pietrinferni et al. 2004) computed for 1.0, 1.1, and 1.2 $M_{\odot}$ stars at the cluster metallicity and assuming the same reddening and a distance modulus quoted above. These tracks bracket the location of our SXPs, thus suggesting a very narrow range for the evolutionary mass, with a mean value $\langle M_{\mathrm{evo}}\rangle = 1.1 \pm 0.1\ M_{\odot}$, which is in excellent agreement with the pulsation estimate. A similar good agreement has been discussed by Gilliland et al. (1998) using the pulsation properties of three mixed-mode SXPs in 47 Tucanae. These authors compared their observations in the Petersen diagram with the same pulsation linear models used here (Santolamazza et al. 2001). However, they also found a significant discrepancy for one of the four analyzed mixed-mode SXPs, which turns out to have a pulsation mass 20% smaller than the evolutionary one.

Recently, a variety of approaches have been used to estimate the mass of BSS stars in globular and open clusters. The first direct measurement of one of the most luminous BSS stars in the core of 47 Tucanae has been presented by Shara et al. (1997) through a spectroscopic analysis of FOS@*HST* data. The derived mass (1.7 $M_{\odot}$) is twice the cluster's MS TO mass and agrees well with the estimate obtained using theoretical stellar evolutionary tracks for a single star. In a subsequent study, using

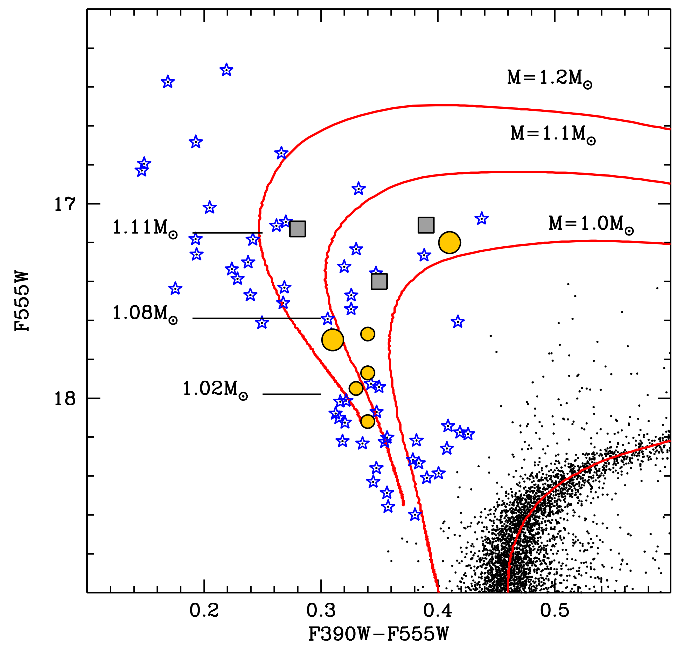

Figure 9. (F555W, F390W−F555W) CMD zoomed in on the BSS region with the SXP BSSs highlighted (symbols as in Figure 6). The size of the symbols reflects the value of the estimated pulsation mass. The horizontal black segments indicate the mean masses (see labels) obtained by grouping the nine SXPs in three bins of increasing magnitude, and they are positioned in correspondence with the mean magnitude of each bin. Evolutionary tracks for single stars with masses equal to 1.0, 1.1, and 1.2 $M_{\odot}$ (from Pietrinferni et al. 2004) are also shown for comparison.

(A color version of this figure is available in the online journal.)

low- and intermediate-resolution spectroscopy in a number of GCs (NGC 6752, NGC 5272, and NGC 6397), De Marco et al. (2005) found that the mean BSS masses for individual clusters (1.27, 1.05, 0.99, and 0.99 $M_{\odot}$, respectively) were significantly lower than the values expected by evolutionary theory. However, this discrepancy can be accounted for by the large errors in their mass evaluations. Only recently, very accurate mass estimates have been possible through spectroscopic and photometric analysis of eclipsing binaries in three GCs, i.e., 47 Tucanae (Thompson et al. 2010), ω Centauri, and NGC 6752 (Kaluzny et al. 2007a, 2007b, 2009), supporting the agreement between these masses and those predicted from single-star evolutionary tracks. The only exception is BSS V209 in ω Centauri, which shows a larger mass ($\sim$0.95 $M_{\odot}$) than MS TO stars ($\sim$0.75 $M_{\odot}$) but smaller than what is expected from the comparison between evolutionary tracks and its bright and blue location in the CMD ($\sim$1.2–1.3 $M_{\odot}$; see Kaluzny et al. 2007a; Ferraro et al. 2006b, for more details). Finally, more recent observations devoted to the study of a double-lined binary BSS in the not-so-young ($\sim$7 Gyr old) open cluster NGC 188 (Geller & Mathieu 2012) indicate that single-star evolutionary models overestimate (by 15% to 30%) the dynamical mass.

While the reasons for some of the observed discrepancies need to be clarified, the results here discussed indicate that single-star evolutionary tracks can be safely used to estimated the BSS mass and suggest values below $\sim$1.2 $M_{\odot}$ for most of the population, in agreement with what has been argued in a number of previous studies (e.g., Ferraro et al. 2006a; Lanzoni et al. 2007). We also note that, for BSSs close to the zero-age MS, masses are more precisely constrained by pulsation models, since stellar evolutionary tracks become degenerate in that region of the CMD.

We conclude the paper by critically discussing the limitations of the adopted approach. The models of Santolamazza et al. (2001) are suitable for radial pulsators. Indeed, the relatively large amplitude of the variations observed ($A_{F555W} \gtrsim 0.05$ mag) and the period ratio measured in double mode pulsators support the hypothesis that most SXPs are radially pulsating stars (as discussed in Stellingwerf 1979). Moreover, despite a linear and nonadiabatic approach to the stellar pulsation, the models have been shown to well reproduce the SXP periods and the blue boundary of the IS (Stellingwerf 1979; Gilliland et al. 1998; Santolamazza et al. 2001). In order to have a full description of the radial stellar pulsation, nonlinear equations have to be solved, including a treatment for the coupling between pulsation and convection. Once available, these models will allow us to address crucial open questions like the dependence of SXP pulsation on masses, luminosities, and chemical content, providing new tools to be used to better constrain the pulsation masses of SXPs. We will have at our disposal more precise PL, period–luminosity–color relations, and, more interestingly, we will be able to accurately predict the amplitudes and the morphology of the SXP light curves. We have started the computation of nonlinear models for SXP stars, extending our theoretical scenario to low masses and for different metallicities. As described in Bono et al. (2002), this requires very long computation time, and results will be presented in forthcoming papers, where we plan to apply this new theoretical approach to all BSSs for which reliable mean magnitudes and periods can be measured.

This research is part of the project Cosmic-Lab (http://www.cosmic-lab.eu) funded by the European Research Council under contract ERC-2010-AdG-267675.

REFERENCES

Arellano Ferro, A., Figuera Jaimes, R., Giridhar, S., et al. 2011, MNRAS, 416, 2265
Bailyn, C. D. 1995, ARA&A, 33, 133
Bellazzini, M., Pasquali, A., Federici, L., Ferraro, F. R., & Pecci, F. F. 1995, ApJ, 439, 687
Bono, G., Caputo, F., Cassisi, S., Castellani, V., & Marconi, M. 1997, ApJ, 479, 279
Bono, G., Caputo, F., Marconi, M., & Santolamazza, P. 2002, in ASP Conf. Ser. 256, Observational Aspects of Pulsating B- and A Stars, ed. C. Sterken & D. W. Kurtz (San Francisco, CA: ASP), 249
Caputo, F., Bono, G., Fiorentino, G., Marconi, M., & Musella, I. 2005, ApJ, 629, 1021
Cardelli, J., Clayton, G., & Mathis, J. 1989, ApJ, 345, 245
Clementini, G., Di Tomaso, S., Di Fabrizio, L., et al. 2000, ApJ, 120, 2054
Da Costa, G. S., Norris, J., & Villumsen, J. V. 1986, ApJ, 308, 743
Dalessandro, E., Ferraro, F. R., & Massari, D. 2013, ApJ, 778, 135
Dalessandro, E., Lanzoni, B., Beccari, G., et al. 2011, ApJ, 743, 11
Dalessandro, E., Lanzoni, B., Ferraro, F. R., et al. 2008, ApJ, 681, 311
De Marco, O., Shara, M. M., Zurek, D., et al. 2005, ApJ, 632, 894
Dotter, A., Sarajedini, A., Anderson, J., et al. 2010, ApJ, 708, 698
Ferraro, F. R., Beccari, G., Dalessandro, E., et al. 2009, Natur, 462, 1028
Ferraro, F. R., Clementini, G., Fusi Pecci, F., & Buonanno, R. 1991, MNRAS, 252, 357
Ferraro, F. R., D'Amico, N., Possenti, A., Mignani, R. P., & Paltrinieri, B. 2001, ApJ, 561, 337
Ferraro, F. R., Fusi Pecci, F., & Bellazzini, M. 1995, A&A, 294, 80
Ferraro, F. R., Fusi Pecci, F., & Buonanno, R. 1992, MNRAS, 256, 376
Ferraro, F. R., Lanzoni, B., Dalessandro, E., et al. 2012, Natur, 492, 393
Ferraro, F. R., Sabbi, E., Gratton, R., et al. 2006a, ApJL, 647, L53
Ferraro, F. R., Sollima, A., Rood, R. T., et al. 2006b, ApJ, 638, 433
Fiorentino, G., Caputo, F., Marconi, M., & Musella, I. 2002, ApJ, 576, 402
Fiorentino, G., Contreras Ramos, R., Clementini, G., et al. 2010a, ApJ, 711, 808
Fiorentino, G., Limongi, M., Caputo, F., & Marconi, M. 2006, A&A, 460, 155
Fiorentino, G., Monachesi, A., Trager, S. C., et al. 2010b, ApJ, 708, 817
Fiorentino, G., Musella, I., & Marconi, M. 2013, MNRAS, 434, 2866
Freire, P. C. C., Wolszczan, A., van den Berg, M., & Hessels, J. W. T. 2008, ApJ, 679, 1433
Geller, A. M., & Mathieu, R. D. 2012, AJ, 144, 54
Gilliland, R. L., Bono, G., Edmonds, P. D., et al. 1998, ApJ, 507, 818
Harris, W. E. 1996, AJ, 112, 1487
Hills, J. G., & Day, C. A. 1976, ApL, 17, 87
Jeon, Y.-B., Lee, M. G., Kim, S.-L., & Lee, H. 2003, AJ, 125, 3165
Jeon, Y.-B., Lee, M. G., Kim, S.-L., & Lee, H. 2004, AJ, 128, 287
Jorgensen, H. E., & Hansen, L. 1984, A&A, 133, 165
Kaluzny, J., Rozyczka, M., Thompson, I. B., & Zloczewski, K. 2009, AcA, 59, 371
Kaluzny, J., Rucinski, S. M., Thompson, I. B., Pych, W., & Krzeminski, W. 2007a, AJ, 133, 2457
Kaluzny, J., Thompson, I. B., Rucinski, S. M., et al. 2007b, AJ, 134, 541
Knigge, C., Leigh, N., & Sills, A. 2009, Natur, 457, 288
Lanzoni, B., Sanna, N., Ferraro, F. R., et al. 2007, ApJ, 663, 1040
Lee, J.-W., & Carney, B. W. 2002, AJ, 124, 1511
Leigh, N., Sills, A., & Knigge, C. 2011, MNRAS, 415, 3771
Leonard, P. J. T. 1989, AJ, 98, 217
Mapelli, M., Ripamonti, E., Tolstoy, E., et al. 2007, MNRAS, 380, 1127
Marconi, M., Fiorentino, G., & Caputo, F. 2004, A&A, 417, 1101
Marconi, M., Musella, I., & Fiorentino, G. 2005, ApJ, 632, 590
Mateo, M., Fischer, P., & Krzeminski, W. 1995, AJ, 110, 2166
Mathieu, R. D., & Geller, A. M. 2009, Natur, 462, 1032
McCrea, W. H. 1964, MNRAS, 128, 147
McNamara, D. H. 2011, AJ, 142, 110
Monelli, M., Cassisi, S., Mapelli, M., et al. 2012, ApJ, 744, 157
Nemec, J. M., Mateo, M., Burke, M., & Olszewski, E. W. 1995, AJ, 110, 1186
Paresce, F., de Marchi, G., & Ferraro, F. R. 1992, Natur, 360, 46
Petersen, J. O. 1978, A&A, 62, 205
Pietrinferni, A., Cassisi, S., Salaris, M., & Castelli, F. 2004, ApJ, 612, 168
Piotto, G., De Angeli, F., King, I. R., et al. 2004, ApJL, 604, L109
Pooley, D., & Hut, P. 2006, ApJL, 646, L143
Pych, W., Kaluzny, J., Krzeminski, W., Schwarzenberg-Czerny, A., & Thompson, I. B. 2001, A&A, 367, 148
Ransom, S. M., Hessels, J. W. T., Stairs, I. H., et al. 2005, Sci, 307, 892
Sandage, A. R. 1953, AJ, 58, 61
Santolamazza, P., Marconi, M., Bono, G., et al. 2001, ApJ, 554, 1124
Shara, M. M., Saffer, R. A., & Livio, M. 1997, ApJL, 489, L59
Stellingwerf, R. F. 1978, ApJ, 224, 953
Stellingwerf, R. F. 1979, ApJ, 227, 935
Stetson, P. B. 1987, PASP, 99, 191
Stetson, P. B. 1994, PASP, 106, 250
Thompson, I. B., Kaluzny, J., Rucinski, S. M., et al. 2010, AJ, 139, 329
Vivas, A. K., & Mateo, M. 2013, AJ, 146, 141
Zinn, R., & Searle, L. 1976, ApJ, 209, 734